

An internally eGFP-tagged α -adaptin is a fully functional and improved fiduciary marker for clathrin-coated pit dynamics

Rosa E. Mino | Zhiming Chen | Marcel Mettlen | Sandra L. Schmid 

Department of Cell Biology, UT Southwestern Medical Center, Dallas, Texas

CorrespondenceSandra L. Schmid, Department of Cell Biology, UT Southwestern Medical Center, Dallas, TX.
Email: sandra.schmid@utsouthwestern.edu**Funding information**

NIH, Grant/Award Number: R01 GM73165

Peer ReviewThe peer review history for this article is available at <https://publons.com/publon/10.1111/tra.12755>.**Abstract**

Clathrin mediated endocytosis (CME) has been extensively studied in living cells by quantitative total internal reflection fluorescence microscopy (TIRFM). Fluorescent protein fusions to subunits of the major coat proteins, clathrin light chains or the heterotetrameric adaptor protein (AP2) complexes, have been used as fiduciary markers of clathrin coated pits (CCPs). However, the functionality of these fusion proteins has not been rigorously compared. Here, we generated stable cells lines overexpressing mRuby-CLCa and/or μ 2-eGFP, σ 2-eGFP, two markers currently in use, or a novel marker generated by inserting eGFP into the unstructured hinge region of the α subunit (α -eGFP). Using biochemical and TIRFM-based assays, we compared the functionality of the AP2 markers. All of the eGFP-tagged subunits were efficiently incorporated into AP2 and displayed greater accuracy in image-based CCP analyses than mRuby-CLCa. However, overexpression of either μ 2-eGFP or σ 2-eGFP impaired transferrin receptor uptake. In addition, μ 2-eGFP reduced the rates of CCP initiation and σ 2-eGFP perturbed AP2 incorporation into CCPs and CCP maturation. In contrast, CME and CCP dynamics were unperturbed in cells overexpressing α -eGFP. Moreover, α -eGFP was a more sensitive and accurate marker of CCP dynamics than mRuby-CLCa. Thus, our work establishes α -eGFP as a robust, fully functional marker for CME.

KEYWORDS

AP2, clathrin-mediated endocytosis, retroviral expression, total internal reflection fluorescence microscopy, transferrin receptor

1 | INTRODUCTION

The uptake of macromolecular cargo into cells plays an essential role in cell physiology. The major entry pathway in mammalian cells is clathrin-mediated endocytosis (CME), a cargo-concentrative, regulated process named after the major coat protein, clathrin.^{1–3} CME is initiated by adaptor proteins that recruit clathrin and recognize cargo receptors to cluster them into growing clathrin coated pits (CCPs).^{4,5} These adaptors, along with other accessory proteins contribute to the

maturation of CCPs. To measure CME in living cells, researchers traditionally use constituents of the clathrin coat conjugated to fluorescent proteins (FPs), coupled with quantitative, live-cell total internal reflection fluorescence microscopy (TIRFM).^{6–9} Custom software enables the accurate detection and tracking of thousands of CCPs and measurement of the rates of CCP initiation, stabilization, growth, and maturation.^{7,10,11}

As the major and defining coat protein, FP-tagged versions of the clathrin light chain (CLC) have proven to be invaluable tools to

This is an open access article under the terms of the Creative Commons Attribution-NonCommercial License, which permits use, distribution and reproduction in any medium, provided the original work is properly cited and is not used for commercial purposes.

measure CCP dynamics.^{8,12} Because CLC must be incorporated with clathrin heavy chains to form functional triskelia, overexpressing CLCs does not affect overall triskelia concentration or the rates of CME. Most studies use eGFP-CLCa, the predominant light chain isoform in nonneuronal cells,¹³ because overexpression of CLCb alters CCP dynamics.¹⁴ A drawback of this marker is that clathrin also functions in vesicle formation from intracellular organelles¹⁵ and forms static structures on endosomes,¹⁶ potentially complicating analysis and interpretation.

An alternative and more selective marker of CME is the AP2 (adaptor protein 2) complex that specifically targets CCP assembly on the plasma membrane (PM).^{17,18} AP2 is a heterotetramer composed of 4 subunits: α , β 2, μ 2, and σ 2.¹⁹ The complex has a globular core formed by all subunits, in which μ 2 and σ 2, at the center, are framed by the two helical solenoid domains of α and β 2. The α and β 2 adaptins also have C-terminal appendage domains connected to their corresponding core regions by unstructured and flexible hinges.^{4,20} The β 2 hinge contains a canonical clathrin-binding box motif (LLNLD),^{21,22} thought to be required for clathrin recruitment and assembly.¹⁹ μ 2, which has two folded domains, μ 2N and μ 2C connected by a flexible linker, undergoes a large conformational change upon AP2 activation²³ in which μ 2C moves away from the core to expose binding sites on μ 2 and σ 2 that recognize endocytic cargo containing tyrosine (Yxx ϕ or NPXY)- and dileucine (D/ExxLL/I or DXLL)-motifs, respectively.²⁴

AP2 complexes are the second most abundant component of the endocytic clathrin coat.^{25,26} Given their specificity as a marker for CME, several FP-tagged AP2 complexes have also been extensively used to track and study CCP dynamics.^{8,27-29} FPs have been fused to both the C-terminus²⁹ and N-terminus²⁸ of the α subunit, the C-terminus of β 2,²⁹ the C-terminus of σ 2,^{8,30} and in an unstructured \sim 110 aa loop extending from within the μ 2C domain.³¹ While in most cases the FP-fused subunits are overexpressed, both μ 2-GFP³² and σ 2-GFP³³⁻³⁵ fusions have also been created by genome-editing proteins. In all cases, the FP-tagged subunits are assumed to be incorporated into holo-AP2 complexes, although the degree of incorporation is rarely reported, but see Cocucci, et al.³⁶ β 2 has its own limitations as it can also be incorporated into AP1 complexes,^{29,37,38} especially when overexpressed. Moreover, overexpressed and isolated β 2 subunits can also be targeted to CCPs.³⁹

Although FP-AP2 fusions have been increasingly used as fiduciary markers of CCPs, comprehensive comparisons of their functionality have not been conducted, yet are essential because of the potential caveats of tagging AP2 subunits. For instance, as a result of their small size and their packing within the AP2 core, tagging the μ 2 and σ 2 subunits may prevent their binding to specific cargo. Moreover, the added size of a tag can impose constraints on motility that could adversely affect conformational changes, leading to the formation of dysfunctional complexes. Previous studies have indeed shown that despite being incorporated into AP2 complexes and being recruited to CCPs, a C-terminally tagged α subunit is unable to rescue CME of transferrin after knockdown of endogenous α .⁴⁰ Other anomalies have also been observed, for example N-terminally tagged α subunit

could not be detected on western blots using anti- α antibodies,²⁸ so the degree of its incorporation into AP2 complexes could not be assessed. Given these concerns, we reasoned that the large (\sim 80aa) unstructured hinge region of α , which has no known binding partners might be an optimal site for generating a functional FP- α fusion.

To be used as an efficient fiduciary marker for CME, FP-tagged subunits should be efficiently incorporated into AP2 complexes that are targeted to CCPs on the PM, should not perturb the kinetics of CME or CCP dynamics compared to the well-established marker FP-CLCa, and should robustly report the dynamic behavior of CCPs. Here, based on these criteria, we rigorously compare the biochemical and functional properties of a new eGFP-tagged α -adaptin with previously employed, but yet incompletely characterized, μ 2-eGFP⁴¹ and σ 2-eGFP^{8,30} subunits. While all three tagged subunits are efficiently incorporated into AP2 complexes, targeted to CCPs and able to report CCP dynamics, only α -eGFP does so without perturbing CME.

2 | RESULTS

To comparatively assess the properties of eGFP-tagged AP2 subunits as faithful markers for CME and CCP dynamics, retroviruses encoding eGFP-tagged α , μ 2 or σ 2 subunits were generated and used to infect human ARPE cells for stable expression. eGFP insertion sites for μ 2 and σ 2 were based on previously published work (Figure 1A,B). Specifically, μ 2-eGFP was derived from an internal HA-tagged rat AP2M1 cDNA obtained from A. Sorkin.⁴¹ eGFP along with a 6-nucleotide LE linker (encoding Leucine and Glutamate) were inserted in-frame downstream of the 11-aa HA tag, which is inserted at aa237 in μ 2. A second LE linker was added at the C-terminus of eGFP followed by the remaining AP2M1 sequence, starting at aa447. σ 2-eGFP was obtained from T. Kirchhausen and encodes an eGFP fusion protein linked to the C-terminus of AP2S1 by a flexible DPPVAT linker.⁸ The linker also encodes a Kozak consensus sequence, which could act a secondary ribosomal binding site (Figure 1A,B). For the α subunit, an eGFP tag was inserted in-frame at aa689 in the unstructured hinge region of a hybrid mouse α subunit construct (see Section 8) obtained from M.S. Robinson (Figure 1A,B).

Two weeks after transduction, cells were FACS-sorted for matching, moderate levels of eGFP expression (Figure 1C). These cells were then allowed to expand for 3 more weeks, and checked by western blot for eGFP-tagged protein expression relative to endogenous levels in parental cells (Figure 1D). At steady state, each subunit was expressed at \sim 2-5-fold higher levels relative to endogenous protein levels observed in the parental wild type cell lines (Endo-). As expected, when the overexpressed eGFP-subunits are incorporated into intact AP2 complexes, the corresponding endogenous subunit are displaced and down-regulated (Figure 1D).

These cell lines were frozen in multiple vials for use in all subsequent analyses. We note that with time in culture, expression levels of tagged subunits decreased (Figure S1A). This was especially true for μ 2-eGFP and σ 2-eGFP, hinting that these constructs might adversely affect cell proliferation so that cells expressing less

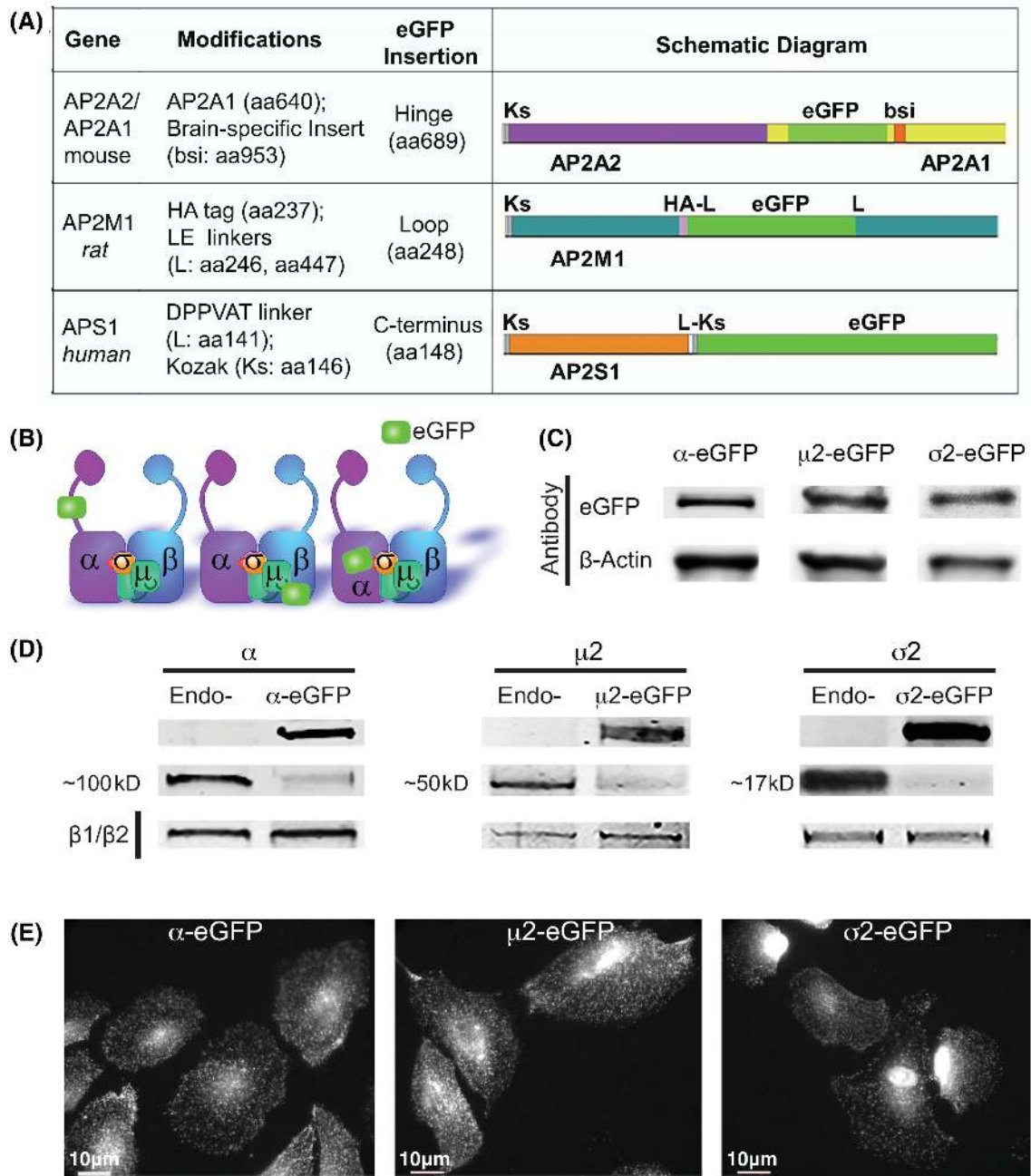


FIGURE 1 Design and validation of cell lines carrying eGFP-tagged AP2 subunits. A, Table with construct details, and their corresponding schematic diagram. Table includes gene name, cDNA species source, modifications made to the protein structure, and site of eGFP insertion. Individual construct diagrams illustrate eGFP insertion, Kozak sequence (Ks), bsi (brain specific insert), linker (L) and Human influenza hemagglutinin tag (HA). B, Illustration of the AP2 protein complex including location of eGFP tag on each construct. C, western blot of stable ARPE cells overexpressing the indicated AP2 subunit using antibodies against GFP and β -actin as loading control. D, Western blot of ARPE cells overexpressing eGFP-tagged AP2 (-eGFP) subunits compared to a parental line expressing only endogenous proteins (Endo-). Antibodies specific to each subunit were used: α MA3-061 with endogenous band at 100 kD, μ 2 in-house with band at \sim 50 kD, and σ 2 ab128950 at \sim 17 kD. E, Immunofluorescence images of cells overexpressing eGFP-tagged AP2 subunits

eGFP-tagged AP2 have a competitive advantage. For this reason, all experiments were done within 4 weeks after thawing.

Epifluorescence imaging of generated cell lines revealed that each of the eGFP-tagged AP2 subunits localized, as expected, to punctate structures at the cell surface (Figure 1E). However, we also detected eGFP fluorescence accumulation in the nucleus of σ 2-eGFP

expressing cells, which could also be seen in earlier publications.⁸ Western blotting of σ 2-eGFP cells revealed significant levels of free-eGFP (Figure S1B), suggesting that this construct is susceptible to cleavage, or that the spurious Kozak sequence at the 5' end of eGFP may enable synthesis independent of σ 2 expression. We favor the latter as we did not detect significant untagged σ 2 in these cells.

3 | α -eGFP, μ 2-eGFP, AND σ 2-eGFP ARE EFFICIENTLY INCORPORATED INTO AP2 COMPLEXES

The first criteria to be met for these tagged AP2 subunits to serve as a robust fiduciary marker for CCPs is their ability to be efficiently incorporated into AP2 complexes. To test this, we first performed eGFP pulldowns using GFP-nAb agarose beads and measured if each eGFP-tagged subunit can pulldown the other subunits of the AP2 tetramer (Figure 2A). Interestingly, we note that overexpression of α -eGFP results in an increase in expression of endogenous μ 2 and σ 2 (Figure 2A, input). Pulldown efficiencies for eGFP-tagged subunits ranged between 76% and 85% (Figure 2B). Quantification of the data (Figure 2C) shows that α -eGFP was able to pulldown $99.3 \pm 7.4\%$ of endogenous μ 2 and $78.8 \pm 0.7\%$ of endogenous σ 2. Similarly, $94.1 \pm 4.2\%$ of available α 2 and $68 \pm 6.3\%$ of σ 2 co-immuno-precipitated with μ 2-eGFP, while 98.7 ± 0.9 of α 2 and

$79.5 \pm 4.1\%$ of endogenous μ 2 co-immuno-precipitated with σ 2-eGFP (Figure 2C). These data establish that endogenous subunits efficiently coassemble with each of the eGFP-tagged subunits to form holo-AP2 complexes.

Given that the eGFP-tagged subunits are overexpressed, we next measured the fraction of tagged subunits incorporated into AP2 complexes. For this, AP2 complexes were pulled-down based on the high affinity binding of β 2 with the C1-domain of ARH (autosomal recessive hypercholesterolemia) using GST-C1-ARH⁴² (Figure 2D, and quantified in Figure 2E,F). Each experiment also included a pulldown using GST alone as bait to check for specificity of signal (Figure S1C). As a control, we measured the efficiency of pulldown of endogenous α 2, μ 2 and σ 2 subunits from parental cell lysates. As antibodies able to distinguish β 1 and β 2 subunits are not available, we were unable to measure the efficiency of pulldown of β 2. However, we found, in nontransfected parent cells that $\sim 80\%$ of α , but only $\sim 50\%$ of μ 2 and σ 2 subunits were pulled down by

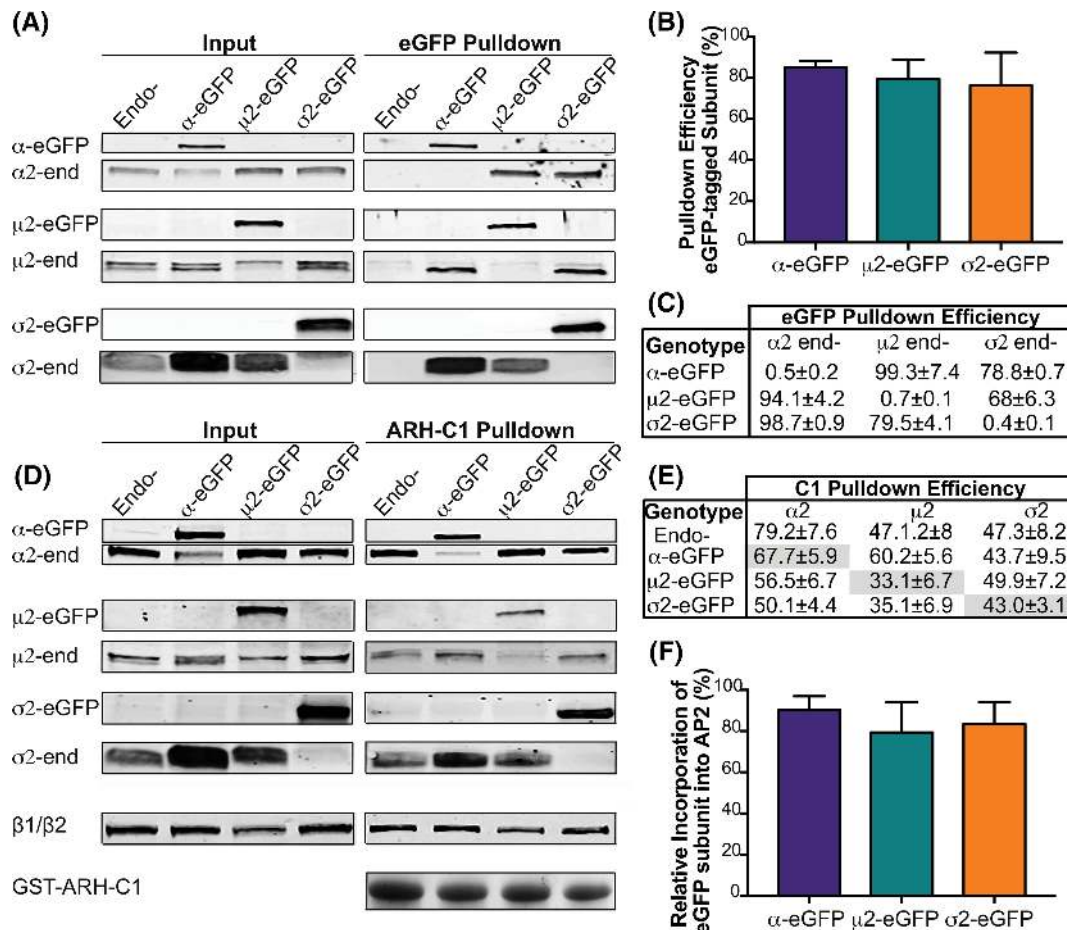


FIGURE 2 α -eGFP, μ 2-eGFP and σ 2-eGFP are efficiently incorporated into AP2 complexes. A, Representative western blot of pulldown of eGFP-tagged subunits using a GFP-trap. Input is 75% of pulldown. Endo- is the parental cell line control. Quantification of pulldown efficiency of eGFP-tagged proteins B, and pulldown efficiency of endogenous (end-) subunits binding to eGFP-AP2 + bead complex, C. Results are an average of 4 experiments and their corresponding SE. D, Representative western blot of AP2 complex pulldowns using C1-ARH-GST, which binds preferentially to β 2. Endo- is the parental cell line. GST-ARH-C1 is visualized in-gel by a trihalo-UV reaction, and the β 1/ β 2 subunits by western blot. E, Quantification of pulldown efficiency for eGFP-tagged (shaded gray), and endogenous AP2 subunits. Results for each graph are averages of $n = 3 \pm$ SE. F, Relative incorporation of tagged subunits into AP2 complexes as a percent of total. Subunit-specific antibodies were used for quantification. Error bars represent SD

GST-C1-ARH, suggesting that even at endogenous levels of expression, the pools of free $\mu 2$ and $\sigma 2$ subunits are higher than of α (Figure 2E). As expected given that they are overexpressed, the percent of each tagged subunit pulled down along with $\beta 2$ was lower than endogenous (Figure 2E, gray). Comparing the pulldown efficiencies in cells expressing tagged subunits relative to endogenous (Figure 2E, Endo-), these data again indicate higher levels of free $\mu 2$ -EGFP and $\sigma 2$ -EGFP than α -EGFP, as might be expected given that other AP2 subunits are selectively upregulated in α -EGFP overexpressing cells. Finally, we quantified the relative incorporation of each eGFP subunit into the AP2 complex, measured as the percentage of tagged subunit over total (tagged/tagged + endogenous $\times 100\%$). Indicative of functionality, each subunit efficiently displaced their endogenous counterpart such that eGFP-tagged species accounted for $90.2 \pm 2.8\%$ of α , $78.4 \pm 7.3\%$ of $\mu 2$ and $83.6 \pm 5.3\%$ $\sigma 2$ subunits in their respective AP2 complexes (Figure 2F). Together, these experiments revealed that α -eGFP, $\mu 2$ -eGFP, and $\sigma 2$ -eGFP are all efficiently incorporated into fully formed AP2 complexes in overexpressing, stable ARPE cells.

4 | α -eGFP, $\mu 2$ -eGFP, AND $\sigma 2$ -eGFP ARE DIFFERENTIALLY TARGETED TO THE MEMBRANE AND INCORPORATED INTO CCPS

The ability of AP2 complexes to be recruited to the PM and trigger CCP assembly depends on a series of activating conformational changes necessary for AP2 targeting to the PM and into CCPs.^{23,43} As these could be impaired by bulk GFP tags, especially in the core $\mu 2$ and $\sigma 2$ subunits, we next compared the ability of AP2 complexes bearing the eGFP-tagged subunits to associate with the PM and colocalize with CCPs. Consistent with the higher cytosolic pools of free $\mu 2$ and $\sigma 2$ subunits detected in our pulldown assays (Figure 2C,E), subcellular fractionation revealed a greater enrichment of α on wild type membrane fractions compared to $\mu 2$ and $\sigma 2$ (Figure 3A,B). However, we observed no significant differences in the enrichment of AP2 complexes bearing either α -eGFP or $\mu 2$ -eGFP in membrane fractions compared to their respective endogenous counterparts (Figure 3A,B). In contrast, the observed ratios for $\sigma 2$ -eGFP were \sim half of that

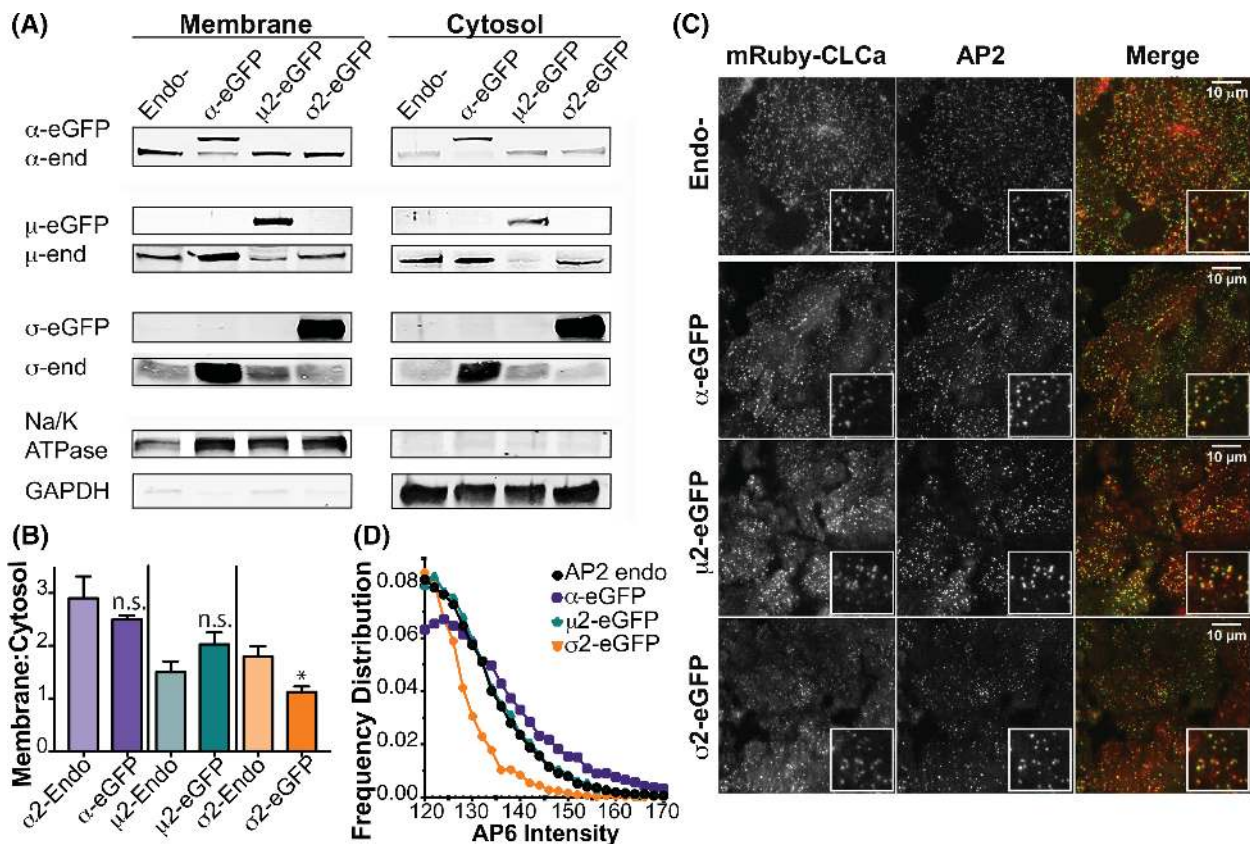


FIGURE 3 α -eGFP, $\mu 2$ -eGFP and $\sigma 2$ -eGFP are targeted to CCPs to membranes and colocalize with clathrin coated pits. A, Representative western blot of fractionation into membrane and cytosolic pools for each ARPE cell line overexpressing eGFP tagged subunits (α -eGFP, $\mu 2$ -eGFP, $\sigma 2$ -eGFP) compared to parental cell line (Endo-). Na/K ATPase was used as a membrane fraction control, and GAPDH as a cytosolic fraction control. Subunit-specific antibodies were used to visualize subunits and for measurements. B, Quantification of membrane to cytosol ratios for each eGFP-tagged subunit (-eGFP) compared to endogenous protein made in the parental cell line (-Endo). Graphed are results from averaging results for three experiments \pm SE. * $P < .05$. C, Upper panel: single plane confocal image of mRuby-CLCa and anti- α AP6 immunostaining. Lower panels, single frames from TIRFM movies of mRuby-CLCa; AP2-eGFP labeled cell lines, showing colocalization of clathrin and AP2 at CCPs. D, Distribution of total AP2 complexes in each cell line by immunostaining and subsequent quantification of AP6 antibody-positive CCPs

observed for its endogenous counterpart. This lower ratio could reflect the high $\sigma 2$ overexpression which allows for an increase in free cytosolic eGFP-tagged subunits. Consistent with this, overexpression of individual eGFP-subunits did not affect the membrane: cytosol ratios of the other endogenous subunits. However, as these differences could not be fully accounted for by the relative incorporation into AP2 complexes, especially comparing $\mu 2$ with $\sigma 2$, these data suggest potential defects in the membrane recruitment of AP2 complexes bearing $\sigma 2$ -eGFP.

Next, we measured the colocalization of AP2-eGFP complexes with clathrin at CCPs using TIRFM (Figure 3C). For this purpose, a parental mRuby-CLCa ARPE cell line was transduced with retroviruses encoding one of the three eGFP-tagged subunits and sorted by FACS to obtain cells uniformly expressing mRuby and eGFP constructs. We examined colocalization of endogenous AP2 with CLCa-mRuby by immunostaining with mAb AP6 (Figure 3C, top panel). TIRFM movies of each double-labeled cell line were obtained and primary/secondary analysis was used to determine the degree of colocalization in bona fide CCPs.⁴⁴ Each of the AP2-eGFP species strongly colocalized ($\sim 90\%$) with mRuby-CLCa labeled CCPs (Figure 3C, bottom three panels, quantified in Figure S2A), indicating that all eGFP-tagged AP2 subunits can support efficient targeting to and assembly of CCPs. However, when the distribution of total AP2 complexes in CLC-positive CCPs was measured by immunofluorescence using anti- α mAb, AP6 (Figure 3D) in the double-labeled cell lines, we found that the majority of $\sigma 2$ -eGFP CCPs have lower AP6 intensities than observed in endogenous control (Figure 3D endo-). Consistent with the data in Figure 3A,B, this suggests that $\sigma 2$ -eGFP-containing AP2 complexes are less efficiently incorporated into CCPs. In contrast, the intensity distribution for AP6 staining at CCPs shifted rightward in cells expressing α -eGFP, indicative of a higher stoichiometry of AP2/CCP and consistent with the slight upregulation of AP2 complexes in these cells.

5 | α -eGFP, UNLIKE $\mu 2$ -eGFP AND $\sigma 2$ -eGFP, DOES NOT PERTURB CCP DYNAMICS

As the main rationale for developing eGFP-tagged AP2 complexes is their use as fiduciary markers to study CCP dynamics, we next performed quantitative live cell TIRFM to compare stable cell lines co-expressing the eGFP-AP2 constructs together with mRuby-CLCa.

We first tested whether the expression of the tagged-AP2 complexes affected mRuby-CLCa dynamics, known to be a robust fiduciary marker of CCPs.⁹ These experiments were performed with dual channel imaging of both mRuby-CLCa and AP2-eGFP constructs, so that AP2 and clathrin dynamics could be studied in the same cells. Initially, using mRuby-CLCa as the primary channel, we examined the earliest AP2-dependent stages of CME, CCP nucleation and stabilization,⁴⁵ which are captured, respectively, by measuring the initiation densities of subthreshold clathrin-labeled structures (sCLSs) and of bona fide CCPs that grow beyond a

user-defined intensity threshold (see Section 8). Neither α -eGFP nor $\sigma 2$ -eGFP expressing cells altered the rates of CCP or sCLS initiation; however, cells expressing $\mu 2$ -eGFP exhibited significantly lower rates of initiation of both CCPs and sCLSs (Figure 4A,B). In all cell lines, the lifetime distributions of mRuby-CLCa-tracked CCPs, expressed as relative frequencies of CCPs for each lifetime, showed the typical Rayleigh-like distribution, reflective of a regulated maturation process. Thus, overexpression of $\mu 2$ -EGFP appears to specifically affect the rates of CCP initiation, whereas later stages of CCP maturation are unaffected. The curves for α -eGFP and $\sigma 2$ -eGFP expressing cells were slightly shifted to the left (Figure 4C), which resulted in small, but significant differences in the median CCPs lifetimes (Figure 4D).

We next examined CCP dynamics in the same cells using the eGFP-tagged AP2 marker as the primary channel. Similar to that observed in mRuby-CLCa experiments, $\mu 2$ -eGFP exhibited significantly lower initiation densities of both bona fide CCPs (Figure 4E) and sCLSs (Figure 4F). Interestingly, in comparing the two CCP markers, we also observed that the initiation densities of both CCPs (~ 0.07 vs $\sim 0.085/\mu\text{m}^2/\text{min}$ for AP2-eGFP vs mRuby-CLCa, respectively) and, especially of sCLSs (~ 0.07 vs $\sim 0.16/\mu\text{m}^2/\text{min}$ for AP2-eGFP vs mRuby-CLCa, respectively) were lower when tracking eGFP-tagged AP2 compared to mRuby-CLCa. The $\sim 2:1$ ratio of sCLSs vs CCPs seen when tracking mRuby-CLCa, likely reflects the detection of single or only a few triskelia that sporadically appear within the TIRF field, as a single triskelion can carry up to 3 mRuby-CLCa and therefore are readily detected given the higher sensitivity of cmeAnalysis.⁴⁴ In contrast, the ratio of sCLSs:CCPs when AP2-eGFP is used as a marker was $\sim 1:1$. This suggests, as expected, that CCP nucleation events bearing AP2 complexes are much more likely to grow and become stabilized and that AP2 complexes more accurately reflect CCP nucleation than clathrin alone. When we analyzed mRuby-CLCa dynamics using DASC (disassembly asymmetry score classification), a new threshold-independent algorithm to distinguish CCPs from abortive coats,¹¹ none of the AP2-eGFP constructs altered the ratio of CCPs:ACs (measured as CCP%) (Figure S2B). Thus, while $\mu 2$ -eGFP expressing cells showed a defect in nucleation, subsequent stabilization of nascent CCPs was unaffected.

The benefit of tracking AP2 complexes over CLCa can clearly be seen when comparing the lifetime distributions of CCPs tracked by the two markers, even though dual channel movies show that $\sim 90\%$ of mRuby-CLCa CCPs are also positive for AP2-eGFP (Figure S2A). Whereas, even above-threshold, bona fide CCPs labeled with mRuby-CLCa exhibit a high frequency of very short-lived (<10 seconds) CCPs (Figure 4C), virtually none are detected with AP2-eGFP markers (Figure 4G). Instead, the lifetime distribution curves of the AP2-eGFP markers drop to zero at the shortest lifetimes. Thus, it is likely that a significant fraction of CLSs identified as bona fide CCPs based on their intensities are AP2-deficient structures. We note that the lifetime distribution of $\sigma 2$ -eGFP labeled CCPs is significantly shifted to the left with a larger population of CCPs with lifetimes <20 seconds compared to $\alpha 2$ - and $\mu 2$ -labeled CCPs (Figure 4G). Correspondingly the median lifetime of $\sigma 2$ -eGFP labeled CCPs is significantly shorter

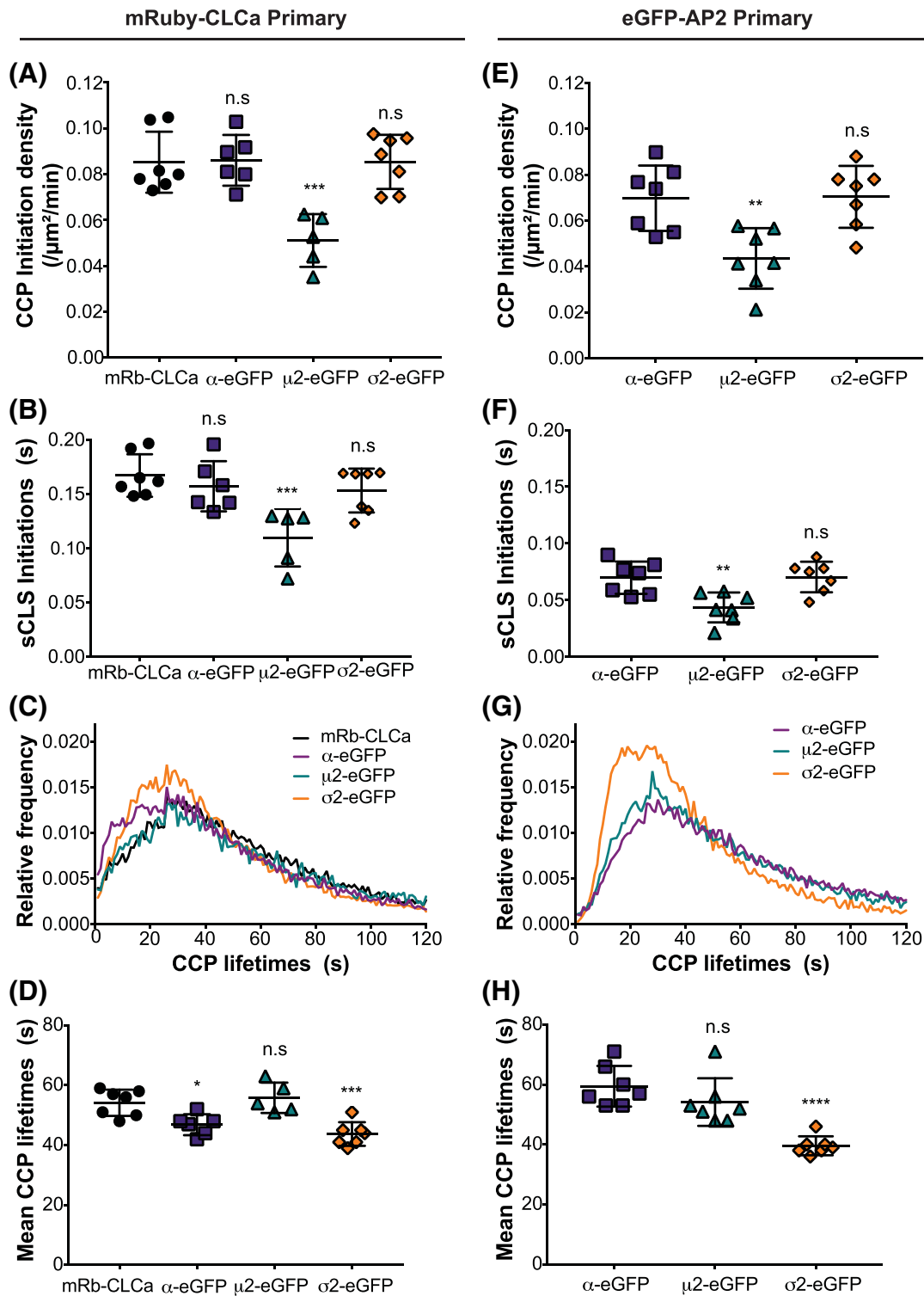


FIGURE 4 α -eGFP is better suited for TIRFM analyses. A-H, Analysis of double-labeled ARPE cells using dual channel TIRFM live-imaging. Cells were seeded at similar density prior to imaging. Each data point is a 7.5-minute movie taken at a 1-second interval per frame. Using cmeAnalysis, we determined CCP dynamics with A-D, mRuby-CLCa and E-H, eGFP-tagged AP2 subunits as the primary channel, see Movies S1-S3, for representative movies from α -eGFP;mRb-CLCa, μ 2-eGFP;mRb-CLCa and σ 2-eGFP;mRb-CLCa cells, respectively. Measurements include: A,E, bona fide clathrin coated pit (CCP) initiation densities, B,F, subthreshold clathrin-labeled structures (sCLS) initiation densities, C,G, CCP lifetime distribution, and D,H, mean lifetime of CCPs analyzed per group. In A-D, mRuby-CLCa experiments, threshold was defined by control mRuby-CLCa cells and applied to other cell lines. eGFP-tagged AP2 subunits were compared by setting the same 40 CCP% as threshold (see Section 8.7). Error bars represent SD with * $P < .05$, ** $P < .01$, *** $P < .001$ and **** $P < .0001$

than for $\alpha 2$ - and $\mu 2$ -labeled CCPs (Figure 4G and H). This suggests that $\sigma 2$ -eGFP labeled CCPs are more likely to abort than $\alpha 2$ - and $\mu 2$ -labeled CCPs. We also observed a slight downward shift in the $\sigma 2$ -eGFP lifetime curve for CCPs between 50 and 120 seconds, suggesting minor perturbations in, or faster CCP maturation. These lifetime defects in $\sigma 2$ -eGFP are consistent with our observations made in fixed cell experiments (Figure 3D) that the $\sigma 2$ -eGFP-expressing cells have fewer AP2 complexes/CCP than those in the other cell lines.

Finally, we compared the average intensity profiles of AP2-eGFPs across lifetime cohorts and observed the characteristic increase in intensity for longer lived CCPs, a plateau phase of AP2 recruitment and a detachment phase (Figure S2C). However, consistent with higher cytosolic pools of both $\mu 2$ - and $\sigma 2$ -eGFP (Figure 3B), the base of their intensity curves (ie, the background) is \sim threefold higher than for $\alpha 2$ -eGFP.

Together these live cell studies demonstrate that both $\mu 2$ -eGFP and $\sigma 2$ -eGFP perturb different aspects of CCP dynamics. They also establish that α -eGFP is a more robust and accurate fiduciary marker of CCP dynamics than mRuby-CLCa.

6 | $\mu 2$ -eGFP AND $\sigma 2$ -eGFP PERTURB TRANSFERRIN RECEPTOR UPTAKE

Finally, we tested the effects of overexpression of each of these tagged AP2 subunits on CME using bulk biochemical assays for internalization. mAb D65 was used as a ligand for transferrin receptors (TfnRs) and biotinylated-epidermal growth factor (B-EGF) as a ligand for the EGF receptor (EGFR) (Figure 5A,B), and endocytosis efficiencies were measured using a previously published In-Cell ELISA (enzyme-linked immunosorbent assay).⁴⁶ Endocytic efficiency was

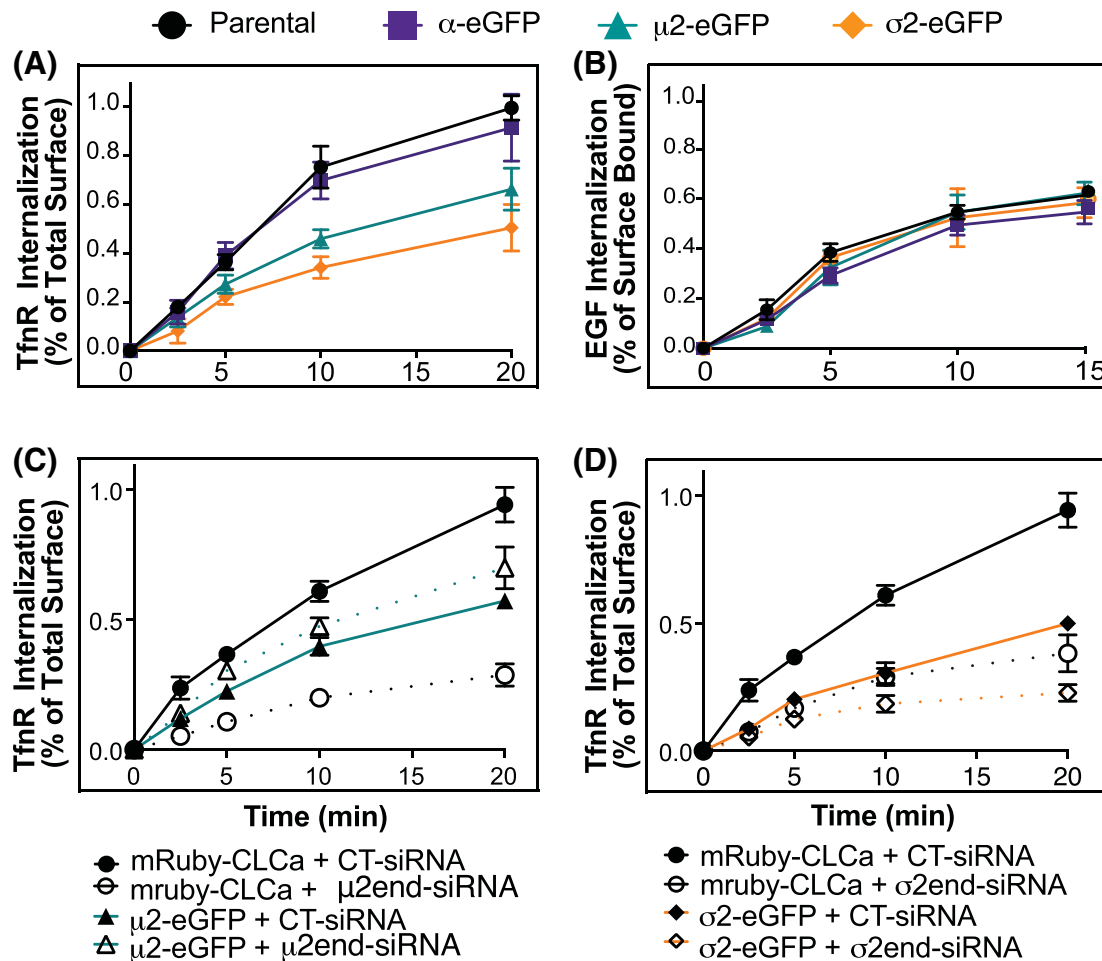


FIGURE 5 Overexpression of $\mu 2$ -eGFP and $\sigma 2$ -eGFP results in inefficient Transferrin uptake. Quantification of internalization efficiency in parental (black), α -eGFP (purple), $\mu 2$ -eGFP (teal) and $\sigma 2$ -eGFP (orange) overexpression cell lines. A, Kinetics of transferrin receptor uptake in ARPE cells, measured using α -TfnR mAb (HTR-D65) as ligand and expressed as a percent of total antibody found at the surface, B, Internalization kinetics of biotin-labeled EGF expressed as a percent of surface-bound. C, Transferrin receptor internalization in mRuby-CLCa; $\mu 2$ -eGFP (teal) cells compared to mRuby-CLCa (black) in the presence of siRNA control (solid lines), or siRNA targeting endogenous $\mu 2$ (dotted lines). D, Transferrin receptor uptake in mRuby-CLCa; $\sigma 2$ -eGFP (orange lines) cells compared to mRuby-CLCa (black) in the presence of siRNA control (solid lines), or siRNA targeting endogenous $\sigma 2$ (dotted lines). Experiments B and C were done together and share the same mRuby-CLCa scrambled control, but were separated for clarity. For all experiments, each data point is the average of three independent experiments. Error bars represent SD

measured as the percent of total surface-bound ligand internalized over time.

The rate of TfnR uptake in ARPE cells expressing α -eGFP was identical to that of the parent, untransduced ARPE cells. However, TfnR internalization was significantly inhibited in both μ 2-eGFP and σ 2-eGFP ARPE cells (Figure 5A). The decrease in the rate of TfnR internalization was accompanied by a corresponding increase in the levels of TfnR on the cell surface (data not shown). Interestingly, the rates of EGF uptake were identical in all of the cell lines tested (Figure 5B). Thus, the effects of μ 2-eGFP and σ 2-eGFP on rates of CME appear to be cargo selective.

Our biochemical analyses showed that while the efficiency of incorporation of α -eGFP into AP2 complexes was \sim 90%, μ 2-eGFP and σ 2-eGFP were incorporated less efficiently such that \sim 20% of AP2 complexes still contain endogenous, untagged subunits. Therefore, we tested the extent to which these endogenous subunits might be supporting CME and CCP dynamics in the μ 2-eGFP- and σ 2-eGFP-expressing cell lines. As expected, using siRNA to selectively target the 5'UTR of endogenous subunits (see Section 8, Figure S3A), knockdown of either μ 2 or σ 2 severely inhibited TfnR uptake in mRuby-CLCa cells that do not express exogenous AP2 subunits (Figure 5C). siRNA knockdown of endogenous μ 2 did not further decrease the rates of TfnR uptake in μ 2-eGFP; however, siRNA knockdown of endogenous σ 2 further inhibited TfnR uptake in σ 2-eGFP-expressing cell lines, suggesting that the remaining endogenous subunit was, in part, contributing to CME efficiency in these cells (Figure 5C,D). In contrast, knockdown of endogenous α 2 in α -eGFP overexpressing cells did not affect TfnR uptake (Figure S3B). Neither siRNA KD of endogenous μ 2 or σ 2 affected the rates of CCP initiation (Figure S3C, E) or the mean CCP lifetimes in (Figure S3 D,F) in the μ 2-eGFP- and σ 2-eGFP-expressing cells. Together these results re-enforce concerns regarding the functionality of both μ 2- and σ 2-eGFP fusion proteins.

7 | DISCUSSION

TIRFM has become a powerful tool to study CME and the dynamic behavior of CCPs. First introduced over 20 years ago,¹² most studies have tracked CCPs by overexpressing fluorescently-tagged CLCa, which are incorporated into clathrin triskelia without affecting their concentration or function.^{6,8,44,47} However, the high sensitivity afforded by the incorporation of up to three copies of eGFP-CLCa/triskelion made it difficult to distinguish small and transient clathrin assemblies from bona fide CCPs.⁴⁴ Moreover, because clathrin also functions on intracellular membranes (eg, endosomes and TGN), these clathrin-labeled structures could complicate analyses. For these reasons, several groups have begun to use fluorescently-tagged subunits of the heterotrimeric AP2 complex, the second most abundant component of CCPs and one that specifically targets CCP assembly at the PM. However, few studies have fully characterized the functionality of these tagged subunits. Here we have compared two commonly used constructs, μ 2-eGFP and σ 2-eGFP with a new construct in which the eGFP tag is incorporated into the unstructured hinge region of

the α -adaptin subunit. While all three fusion proteins are efficiently incorporated into AP2 complexes when stably overexpressed at \sim 2-5-fold over endogenous levels, we find that only α -eGFP is fully functional. Indeed, α -eGFP proved to be a more robust and accurate fiduciary marker of bona fide CCPs than eGFP-CLCa.

In all cases, the overexpressed AP2 subunits displaced their endogenous counterparts and were efficiently incorporated into intact AP2 complexes. Interestingly, overexpression of α -eGFP resulted in the upregulation of both μ 2 and σ 2 subunits, and correspondingly increased the concentration of AP2 at CCPs. Whether the increase in μ 2 and σ 2 expression occurred at the transcription level and/or at the level of protein stabilization remains to be determined.

The most commonly used fluorescently-tagged AP2 subunit, first introduced by Kirchhausen and colleagues⁸ is the C-terminally tagged σ 2-eGFP. Indeed, this subunit has been endogenously tagged in SUM159 breast cancer cells.³³⁻³⁵ However, and in agreement with previous studies,³⁴ we find that σ 2-eGFP expressing cells exhibit impaired rates of TfnR uptake, as well as altered CCP dynamics, including increased numbers of short-lived, presumably late abortive CCPs, and altered maturation rates. While it is possible that the shift in lifetime distribution of σ 2-eGFP labeled coated pits represents more rapid maturation, we think this is unlikely given the defects in CME we observed. Furthermore, consistent with impaired CME, ARPE cells rapidly lose expression of σ -eGFP over time in culture. Interestingly, we also found that \sim 50% of endogenous σ 2 and \sim 60% of overexpressed σ 2-eGFP subunits are not incorporated into AP2 complexes, nor targeted to membranes. Whether this residual σ 2 exists as free monomers or is incorporated into other complexes remains to be determined. Finally, the σ 2-eGFP construct we used encodes an internal Kozak sequence and we detect free eGFP that likely accounts for the nuclear-localized fluorescent signal that we and others⁸ detect in cells overexpressing σ 2-eGFP. This issue has now been corrected in genome-edited cells carrying an eGFP tag in the same region of σ 2.³⁴ Based on our data, we conclude that σ 2-eGFP is not a robust fiduciary marker of CCP dynamics, and hence results stemming from its use should be interpreted with caution.

The μ 2-eGFP fusion generated by incorporating eGFP into the flexible loop in μ 2C is also not fully functional. Previous studies had shown that μ 2 bearing an HA or Myc epitope at this location was able to support efficient Tfn uptake^{40,41,45}; thus, it seemed reasonable to place an eGFP tag at the same location. However, cells expressing μ 2-eGFP exhibited reduced TfnR uptake, and reduced initiation densities of both sCLSs and CCPs. This is not entirely surprising as internally tagging other μ subunits can perturb their function.⁴⁸ As for σ 2-eGFP, with time in culture, the μ 2-eGFP cells also lost expression more rapidly when compared to cells expressing α -eGFP. Interestingly, eGFP has been inserted into the same site in endogenous μ 2 by genome-editing a subset of alleles in the polyploid MDA-MB-231 cell line and used to distinguish "authentic" from "false" CCPs.³² However, despite \sim 50% knock-in efficiency as assessed by PCR, the levels of expression of μ 2-eGFP in most of the cell lines generated and studied corresponded to a fraction of untagged endogenous protein (see fig. S5E in Reference 32), consistent with perturbed function of the

tagged subunit. The efficiency of incorporation into AP2 complexes was not assessed. Based on our data, it is unlikely that this construct is fully functional. Nevertheless, we cannot rule out differences between cell types, the linkers used (although not specified), nor the possibility that compensatory mechanisms arose during clonal selection to restore efficient CME.

The endocytosis defect seen for both σ 2-eGFP and μ 2-eGFP cells was cargo selective, in that EGF uptake, which has been shown to be less AP2-dependent,^{49,50} and can be mediated by alternative non-clathrin pathways, was unaffected. This was expected, as other FP-tagged versions of μ 2 also did not exhibit EGFR traffic defects.^{31,51} Moreover, there is evidence in the literature of endogenously eGFP tagged σ 2 exhibiting mild defects in endocytosis of chimeras bearing YAAL or EAAALL but not FANPAY, further reinforcing the idea that defects arising from the introduction of these tags may be a cargo-selective issue.³⁴ As both σ 2 and μ 2 are directly involved in cargo recognition, the bulky eGFP tags on the core AP2 subunits may impair this function.

Our findings establish α -eGFP as a robust and accurate fiduciary marker of CCPs. The unstructured hinge region of α adaptin has no known binding partners. Its unstructured length (~80 aa) is thought to enable the attached α -appendage domain to flexibly interact with numerous endocytic accessory proteins during CCP stabilization and maturation.²⁰ This flexibility perhaps accounts for our findings that insertion of an eGFP moiety does not interfere with AP2 function. Indeed, the rates of assembly and maturation of α -eGFP labeled CCPs are indistinguishable from mRuby-CLCa labeled CCPs. The exception being that >twofold fewer short-lived, dim (ie, subthreshold) structures are detected and lifetime distribution curves are no longer populated by very short-lived (<10 seconds) CCPs. These data suggest that AP2-labeled structures more accurately track bona fide CCPs.

Using genome-edited fluorescent tags in imaging studies has clear advantages because of the lack of excess signal resulting from overexpression, although this problem is mitigated when subunits of obligate heterologomers are tagged. However, in this work we intentionally used retroviral vectors to generate overexpressing stable cell lines as a more versatile tool to study CCP dynamics. Stable cell lines were generated because overexpression studies using transient transfection does not allow sufficient time to replace endogenous AP2 subunits.³⁹ More importantly, the ability to sort for cells mildly overexpressing fluorescently-tagged AP2 subunits increases the likelihood of their efficient incorporation into intact AP2 complexes. Use of retroviral-driven overexpression of eGFP-tagged markers rather than editing the endogenous locus allows for more rapid generation of labeled cells and greater versatility as the viral constructs are readily applicable to multiple cell lines. This approach also enables analysis of cell lines that are difficult to genome edit and/or that cannot be grown from single cell clones, including the ARPE cells used herein. Moreover, when amplifying cells during clonal selection after genome editing, compensatory mechanisms can emerge and be selected for, allowing cells adapt to the possibly perturbed function of tagged proteins. Having identified α -eGFP as a robust and functional marker of CCPs, genome-edited cells or organisms in which eGFP is inserted

into this site in the endogenous locus are likely to be excellent tools for analysis of CME. However, as AP2 has two isoforms, identifying which isoform, AP2A1 or AP2A2, is predominantly expressed in the cell of choice will be important. Again, mildly overexpressing a single, nonfunction-perturbing α isoform is an easier proposition.

Altogether, our findings point to the importance of careful biochemical and functional characterization of fluorescently-tagged CCP markers. They also establish that mild and stable overexpression of our α -eGFP construct can serve as a robust and accurate fiduciary marker for CCP dynamics.

8 | METHODS

8.1 | Generation of constructs

All eGFP-tagged AP2 constructs were generated by seamless cloning techniques and subcloned into a modified pMIB6 retroviral vector. To avoid background, the BFP and the IRES sequences were removed from the original PMIB6 backbone using primers:

5'-AGCGGCCGCTCGAGATCCTCCGGACTCAGATCC-3'
5'-GGATCTGAGTCCGGAGGATCTCGAGCGGCCGCT-3'.

α -eGFP was designed as a chimeric protein based on a mouse cDNA construct gifted, and previously described, by the Robinson lab.⁴⁰ Briefly, the 3' section of AP2A2 cDNA was removed using a Clal site, and replaced by the corresponding AP2A1 region (aa640), which includes a brain-specific insert (bsi; aa953). eGFP was inserted by seamless cloning into aa689, which corresponds to the hinge region of α . 5' sequences were also modified to confer siRNA resistance.⁴⁰

To generate μ 2-eGFP, eGFP was inserted into the loop region (aa248) of rat AP2M1 cDNA preceded by an HA-tag as described in previous work.⁴¹ There are two short linkers (LE) at each end of eGFP (aa 246, 447).

σ 2-eGFP was generated from a construct gifted to us by the Kirchhausen lab.⁸ This construct carries eGFP at the C-terminus of AP2S1 following a linker (DPPVAT), and a secondary Kozak sequence.

To subclone α , μ 2 and σ 2 sequences into the modified PMIB6 vector, the following primers were used:

α insert specific primers

FWD 5'-CCGTAGGCATGGTGAGCAAGGGC-3'
REV 5'-AGGTTCCCGGACTTGTACAGCTCG-3'

α vector specific primers

FWD 5'-ACAAGTCCGGGAACCTCCTGGTG-3'
REV 5'-CTCACCATGCTACGGGAGCCGG-3'

μ 2 insert specific primers.

FWD 5'-TCGCCACCATGATCGGAGGCTTATTCATCTATAATCAC-3'
REV 5'-TCTGAGTCCGGACTAGCAGCGGGTTTCGTAATG-3'

μ 2 vector specific primers

FWD 5'-GCTGCTAGTCCGGACTCAGATCCGTCGAC-3'
REV 5'-TCCGATCATGGTGCGAATCCCGGATCC-3'

σ insert specific primers

FWD 5'-TCGCCACCATGATCCGATTCATTCTCATCCAGAAC-3'

REV 5'-TCTGAGTCCGATTACTTGACAGCTCGTCCATGCC-3'

σ vector specific primers

FWD 5'-CTGTACAAGTAATCCGGACTCAGATCCGTCGAC-3'

REV 5'-AATCGGATCATGGTGGCGAATTCGCGATCC-3'

Each construct was then transfected into HEK293FT to collect generated retrovirus 48 hours later.

8.2 | Cell culture, viral infection and siRNA knockdown

Parental human retinal pigmented epithelium (ARPE-19) cells obtained from ATCC were used to generate stable cell lines. All cells were cultured in DMEM/F12 supplemented with 10% FBS at 37°C in a 5% CO₂ atmosphere.

Stable ARPE cell lines carrying fluorescently-tagged CLCa were generated as previously described.⁴⁴ eGFP-labeled AP2 stable cells lines were generated by transducing ARPE cells with the corresponding retrovirus. After 72 hours, cells were isolated in populations with different eGFP expression levels by fluorescence-activated cell sorting (FACS Moody Foundation Flow Cytometry, UTSW). Cells exhibiting equivalent over-expression of eGFP-tagged AP2 subunits at ~5 times that of endogenous were then allowed to grow for 3 weeks, frozen and used as stocks.

siRNA transfection was conducted in DMEM/F12 by supplementing Opti-MEM with Lipofectamine RNAi-MAX (Invitrogen 13778150). Cells were added to a 6-well plate (200,000 cells/well), and a mix of siRNA and RNAi-MAX was added dropwise while shaking the plate. Two rounds of siRNA were carried out through 5 days to achieve over 90% target protein knockdown. Sequences used for knockdown of endogenous α , μ 2 and σ 2 are below. For knockdown of μ 2, both target sequences were used. μ 2 and σ 2 target sequences are found at the 5'UTR. α 2 has been previously reported.⁴⁶ Knockdown levels were then checked by western blot.

Endogenous α 5'-GAGCAUGUGCACGUGGCCA-3'

Endogenous σ 2 5'-CTTCGTGGAGGTCTTAAACGA-3'

Endogenous μ 2-1 5'-GTGTGACTTCGTCCAGTTACA-3'

Endogenous μ 2-2 5'-GGGATAGTGTGAGCTTCATTT-3'

8.3 | Endocytosis (uptake) assay

Uptake of TfnR and EGF was measured by already established in-cell ELISA protocols.⁴⁶ In brief, 16,000 cells per well were seeded in 96-well plates (Costar #9102) and left to attach for 16 hours at 37°C. Prior to each assay the cells were washed and media replaced with PBS4+ (1 mM CaCl₂, 1 mM MgCl₂, 0.2% BSA, 5 mM D-glucose in 1xPBS) for starvation at 37°C for 30 minutes. A subset of cells was then placed at 4°C, and media was replaced with cold PBS4+ for surface-bound measurements and blank controls, while timepoints

were incubated in a 37°C water bath. PBS4+ containing: 5 mg/mL of HTR-D65 (anti-TfnR mAb) or 20 ng/mL Biotin-EGF (Sigma) was then added for the indicated times. A subset of cells was kept at 4°C for surface-bound measurements and blank controls while timepoints were incubated in a 37°C water bath for the indicated time. Cells at 37°C and blanks were then washed with cold acidic media (0.2 M acetic acid, 0.2 M NaCl, pH 2.3) to remove surface-bound antibodies, followed by washing with cold PBS. All cells were then fixed in 4% formaldehyde (Electron Microscopy Sciences) for 5 minutes at 4°C, and followed by 25 minutes at 37°C. All wells were then washed 2x in PBS, followed by a 0.1% Triton-X in PBS wash for permeabilization. We then proceeded to block the wells with Q-PBS (2% BSA, 0.1% lysine, 0.01% saponin in PBS, pH 7.4) for 15 minutes, followed by a second round of blocking with 5%BSA/2%casein, or 2% casein only for EGF uptake, in PBS for 1 hour. After blocking, the cells were washed 1x with PBS and the corresponding HRP-conjugated antibody was added and incubated overnight (anti-mouse secondary for HTR-D65 or Streptavidin-POD for Biotin-EGF, Sigma). Secondary antibodies were then removed by 6 PBS washes. OPD developing solution was used to obtain colorimetric read out by measuring absorbance at 490 nm (Biotek Synergy H1 Hybrid Reader). Well-to-well variability in cell number was normalized by a BCA assay (Thermo Fisher Scientific). Internalized ligand was expressed as the percentage of the total surface-bound ligand at 4°C (ie, without acid wash step), measured in parallel.

8.4 | Immunoprecipitations and subcellular fractionation

cDNA encoding the GST-tagged C1-Autosomal Recessive Hypercholesteremia (GST-C1-ARH) was a generous gift of Linton Traub. GST-C1-ARH protein expression and purification were performed as previously described.⁴² GST only control was included in every experiment.

For GST-pulldowns, 1 × 10⁶ ARPE cells were lysed in HEPES buffer (100 mM HEPES, 0.2 mM EGTA, 0.5 mM MgCl₂, 1% NP-40, 50 mM NaCl, 1x protease inhibitor, 1x phosphatase inhibitor or sodium orthovanadate, pH = 7.4), spun at 500 g for 5 minutes to remove nuclei, and checked for concentration by standard BCA methods. Equivalent amounts of protein for each sample were added to Glutathione beads saturated with GST-C1-ARH, and rotated overnight at 4°C. Samples were then washed with HEPES buffer to remove excess unbound protein, resuspended and eluted at 90°C for 5 minutes with SDS sample loading buffer.

Pulldown of eGFP was performed using GFP-nAb agarose beads (Allele Biotech) following the instructions provided by the manufacturer, with lysate prepared and analyzed as described above.

For fractionation experiments 1.2 × 10⁶ ARPE cells per genotype were detached with 10 mM EDTA at 37°C, neutralized with 100 mM MgCl₂, washed in 1xPBS, and resuspended in 500 μ L of cold fractionation lysis buffer (25 mM HEPES, 250 mM sucrose, 1 mM MgCl₂, 2 mM EGTA, pH = 7.4). Cells were lysed by 6 rounds of rapid freeze-thaw cycles followed by 3 × 10 seconds water-sonication pulses. Cells were then spun at 500 g for 3 minutes to remove nuclei, and supernatant was transferred to tubes for ultracentrifugation. One hundred

micro liter were kept as input samples. Samples were then spun at 110 000 g for 30 minutes. Resulting supernatant was collected and TCA-precipitated by standard methods. Both pellet and supernatant were resuspended in sample buffer. Samples were heat denatured in sample buffer and analyzed by SDS-PAGE and western blotting.

Following standard semi-dry western blot methods, the following antibodies were used to visualize proteins: MA3-061 for $\alpha 2$ (Thermo Fisher), in-house and Abcam ab106542 for $\mu 2$, Abcam, ab128950 for $\sigma 2$, Sigma A4450 for $\beta 1/\beta 2$, Abcam ab76020 for Na/K ATPase, Santa Cruz SC-25778 for GAPDH, Santa Cruz SC138 for GST, in-house 4879 for CLCa. General loading controls were β -actin, $\beta 1/2$, trihalo-UV gels (Stainfree BioRad), and Coomassie blue staining.

8.5 | Immunofluorescence

Cells were seeded on 0.1 mg/mL gelatin-coated 22 × 22 mm glass (Corning, #2850-22) overnight, rinsed three times in 1×PBS and fixed for 2 minutes at 37°C with a mix of 0.5% Triton-X100 and 2% formaldehyde (in PBS), followed by a fixation in 4% formaldehyde for 30 minutes at 37°C. Subsequently, cells were blocked with Q-PBS without saponin for 30 minutes. Primary and secondary antibodies were diluted in Q-PBS. Primary antibodies used were: HTR-D65 (Tfn 1:500), CLCa (1:1000 4879 in-house), AP6 (α -adaptin mAb 1:500). Corresponding secondary labeled antibodies were used at 1:1000. Cells were mounted on slides with Fluoromount-G.

8.6 | Microscopy and imaging

TIRFM was performed as previously described.¹⁴ Briefly, 22x22mm coverslips were acid-washed and coated with 0.2 mg/mL gelatin (Corning, #2850-22). For all imaging, a 60x Nikon 1.49 NA TIRFM DIC objective (Nikon) was used combined with an additional 1.8× tube lens (yielding a final magnification of 108×), mounted on a Ti-Eclipse inverted microscope with Perfect Focus System (Nikon). TIRFM illumination was achieved using an Andor “Discovery Platform/borealis widefield illuminator.” Time-lapse series were acquired at a penetration depth of 80 nm and a frame rate of 1 Hz using a PCO-Edge 5.5 sCMOS camera. During imaging, cells were maintained at 37°C in DMEM/F12 supplemented with 10% fetal bovine serum.

Confocal images were acquired with a similar setup as described above, using a 50 μ m pinhole disk and an Andor Zyla 4.2 sCMOS camera.

Both microscopes have a custom-built full body environmental chamber with temperature control and CO₂ stage incubator operated by Bold Line controller and OKO-Touch with SmartBox for data logging, and Molecular Devices MetaMorph software.

8.7 | Quantification and statistical analysis

Experiments were performed with biological replicates and the data presented are average values \pm standard deviations. The intensity of

protein blots was analyzed with the Syngene (chemoluminescence) and ImageStudio (LICOR Odyssey) softwares. Results are described as average values \pm standard deviations or error of the mean, where indicated. The statistical significance was analyzed by two-tailed Student's *t*-test or One-way ANOVA in Prism 7. Significance is described as follows, $P < .05$; $P < .01$; $P < .001$; $P < .0001$.

When cmeAnalysis was used to quantify CCP dynamics using mRuby-CLCa as the primary channel, intensity threshold was set to remove the large population of transient structures⁴⁴ and applied to all conditions imaged on the same day. When AP2-eGFP was tracked as the primary channel, we were unable to use the same threshold because of intensity and behavioral differences between the independent cell lines. Instead, we assessed the dynamic properties of CCPs (tracked in the same cells using mRuby-CLCa as the primary channel) using DASC (Disassembly Asymmetry Score Classification), a recently developed computational pipeline that distinguishes abortive coats from bona fide CCPs in an unbiased and intensity threshold-independent manner,¹¹ and determined the appropriate % of CCPs ($40 \pm 3\%$), which was used to set the thresholding for cmeAnalysis for all cells. For TIRFM data, statistical significance was analyzed by two-tailed Student's *t*-test. *, $P < .05$; **, $P < .005$; ***, $P < .005$.

9 | CODE

The cmeAnalysis code package used for data analyses in this work is well-established from previous work by our lab.^{7,10,44,52} A detail description and validation of the DASC analysis methods can be found in Wang et al.¹¹

ACKNOWLEDGMENTS

We thank Dr. Zuzana Kadleková for reagents, Dr. Emanuele Cocucci for manuscript comments, and Dr. Ashley Lakoduk for reagents and help with manuscript preparation. We also thank the FACS core facility at the UTSW Children's Research Center, Heather Grossman for help with sample generation, retrovirus production, and analysis, and Aparna Mohanakrishnan for technical support in PCR. We thank Dr. Ashley Lakoduk and Dr. Madhura Bhavé for helpful discussion. This work is supported by NIH R01 GM73165 to Sandra L. Schmid and Marcel Mettlen.

CONFLICT OF INTEREST

The authors declare no conflict of interest.

AUTHOR CONTRIBUTIONS

Rosa E. Mino, Marcel Mettlen and Sandra L. Schmid designed the experiments, interpreted the results. Rosa E. Mino, Zhiming Chen and Marcel Mettlen performed TIRFM imaging and data analysis. Rosa E. Mino performed all other experiments.

ORCID

Sandra L. Schmid  <https://orcid.org/0000-0002-1690-7024>

REFERENCES

1. Kaksonen M, Roux A. Mechanisms of clathrin-mediated endocytosis. *Nat Rev Mol Cell Biol.* 2018;19(5):313-326.
2. McMahon HT, Boucrot E. Molecular mechanism and physiological functions of clathrin-mediated endocytosis. *Nat Rev Mol Cell Biol.* 2011;12(8):517-533.
3. Mettlen M, Chen P-H, Srinivasan S, Danuser G, Schmid SL. Regulation of Clathrin-mediated endocytosis. *Annu Rev Biochem.* 2018;87:871-896.
4. Owen DJ, Collins BM, Evans PR. Adaptors for clathrin coats: structure and function. *Annu Rev Cell Dev Biol.* 2004;20:153-191.
5. Traub LM, Bonifacino JS. Cargo recognition in clathrin-mediated endocytosis. *Cold Spring Harb Perspect Biol.* 2013;5(11):a016790.
6. Merrifield CJ, Feldman ME, Wan L, Almers W. Imaging Actin and dynamin recruitment during invagination of single clathrin-coated pits. *Nat Cell Biol.* 2002;4(9):691-698.
7. Loerke D, Mettlen M, Yarar D, et al. Cargo and Dynamin regulate Clathrin-coated pit maturation. *PLoS Biol.* 2009;7(3):e1000057.
8. Ehrlich M, Boll W, van Oijen A, et al. Endocytosis by random initiation and stabilization of Clathrin-coated pits. *Cell.* 2004;118(5):591-605.
9. Mettlen M, Danuser G. Imaging and modeling the dynamics of clathrin-mediated endocytosis. *Cold Spring Harb Perspect Biol.* 2014;6(12):a017038.
10. Jaqaman K, Loerke D, Mettlen M, et al. Robust single-particle tracking in live-cell time-lapse sequences. *Nat Methods.* 2008;5(8):695-702.
11. Wang X, Chen Z, Mettlen M, Noh J, Schmid SL, Danuser G. DASC, a sensitive classifier for measuring discrete early stages in clathrin-mediated endocytosis. *elife.* 2020;9:e53686.
12. Gaidarov I, Santini F, Warren RA, Keen JH. Spatial control of coated-pit dynamics in living cells. *Nat Cell Biol.* 1999;1(1):1-7.
13. Acton SL, Brodsky FM. Predominance of clathrin light chain LCb correlates with the presence of a regulated secretory pathway. *J Cell Biol.* 1990;111(4):1419-1426.
14. Chen PH, Bendris N, Hsiao YJ, et al. Crosstalk between CLCb/dyn1-mediated adaptive Clathrin-mediated endocytosis and epidermal growth factor receptor signaling increases metastasis. *Dev Cell.* 2017;40(3):278-288.
15. Brodsky FM, Chen CY, Knuehl C, Towler MC, Wakeham DE. Biological basket weaving: formation and function of clathrin-coated vesicles. *Annu Rev Cell Dev Biol.* 2001;17:517-568.
16. Norris A, Grant BD. Endosomal microdomains: formation and function. *Curr Opin Cell Biol.* 2020;65:86-95.
17. Pearse BMF, Robinson MS. Clathrin, adaptors, and sorting. *Annu Rev Cell Biol.* 1990;6(1):151-171.
18. Robinson MS. Assembly and targeting of adaptin chimeras in transfected cells. *J Cell Biol.* 1993;123(1):67-77.
19. Kirchhausen T, Owen D, Harrison SC. Molecular structure, function, and dynamics of clathrin-mediated membrane traffic. *Cold Spring Harb Perspect Biol.* 2014;6(5):a016725.
20. Praefcke GJK, Ford MGJ, Schmid EM, et al. Evolving nature of the AP2 alpha-appendage hub during clathrin-coated vesicle endocytosis. *EMBO J.* 2004;23(22):4371-4383.
21. Shih W, Gallusser A, Kirchhausen T. A clathrin-binding site in the hinge of the beta 2 chain of mammalian AP-2 complexes. *J Biol Chem.* 1995;270(52):31083-31090.
22. ter Haar E, Harrison SC, Kirchhausen T. Peptide-in-groove interactions link target proteins to the beta-propeller of clathrin. *Proc Natl Acad Sci U S A.* 2000;97(3):1096-1100.
23. Jackson LP, Kelly BT, McCoy AJ, et al. A large-scale conformational change couples membrane recruitment to cargo binding in the AP2 clathrin adaptor complex. *Cell.* 2010;141(7):1220-1229.
24. Kelly BT, Owen DJ. Endocytic sorting of transmembrane protein cargo. *Curr Opin Cell Biol.* 2011;23(4):404-412.
25. Kirchhausen T. Adaptors for clathrin-mediated traffic. *Annu Rev Cell Dev Biol.* 1999;15:705-732.
26. Robinson MS, Bonifacino JS. Adaptor-related proteins. *Curr Opin Cell Biol.* 2001;13(4):444-453.
27. Bucher D, Frey F, Sochacki KA, et al. Clathrin-adaptor ratio and membrane tension regulate the flat-to-curved transition of the clathrin coat during endocytosis. *Nat Commun.* 2018;9(1):1109.
28. Rappoport JZ, Simon SM. A functional GFP fusion for imaging clathrin-mediated endocytosis. *Traffic.* 2008;9(8):1250-1255.
29. Keyel PA, Watkins SC, Traub LM. Endocytic adaptor molecules reveal an endosomal population of clathrin by total internal reflection fluorescence microscopy. *J Biol Chem.* 2004;279(13):13190-13204.
30. Fan L, Hao H, Xue Y, et al. Dynamic analysis of Arabidopsis AP2 σ subunit reveals a key role in clathrin-mediated endocytosis and plant development. *Development.* 2013;140(18):3826-3837.
31. Huang F, Jiang X, Sorkin A. Tyrosine phosphorylation of the beta2 subunit of clathrin adaptor complex AP-2 reveals the role of a dileucine motif in the epidermal growth factor receptor trafficking. *J Biol Chem.* 2003;278(44):43411-43417.
32. Hong SH, Cortesio CL, Drubin DG. Machine-learning-based analysis in genome-edited cells reveals the efficiency of Clathrin-mediated endocytosis. *Cell Rep.* 2015;12(12):2121-2130.
33. Kural C, Akatay AA, Gaudin R, et al. Asymmetric formation of coated pits on dorsal and ventral surfaces at the leading edges of motile cells and on protrusions of immobile cells. *Mol Biol Cell.* 2015;26(11):2044-2053.
34. Aguet F, Upadhyayula S, Gaudin R, et al. Membrane dynamics of dividing cells imaged by lattice light-sheet microscopy. *Mol Biol Cell.* 2016;27(22):3418-3435.
35. Pascolutti R, Algisi V, Conte A, et al. Molecularly distinct Clathrin-coated pits differentially impact EGFR fate and signaling. *Cell Rep.* 2019;27(10):3049-3061 e3046.
36. Cocucci E, Aguet F, Boulant S, Kirchhausen T. The first five seconds in the life of a clathrin-coated pit. *Cell.* 2012;150(3):495-507.
37. Page LJ, Robinson MS. Targeting signals and subunit interactions in coated vesicle adaptor complexes. *J Cell Biol.* 1995;131(3):619-630.
38. Sorkina THF, Beguinot L, Sorkin A. Effect of tyrosine kinase inhibitors on clathrin-coated pit recruitment and internalization of epidermal growth factor receptor. *J Biol Chem.* 2002;277(30):27433-27441.
39. Edeling MA, Mishra SK, Keyel PA, et al. Molecular switches involving the AP-2 β 2 appendage regulate Endocytic cargo selection and Clathrin coat assembly. *Dev Cell.* 2006;10(3):329-342.
40. Motley AM, Berg N, Taylor MJ, et al. Functional analysis of AP-2 alpha and mu2 subunits. *Mol Biol Cell.* 2006;17(12):5298-5308.
41. Nesterov A, Carter RE, Sorkina T, Gill GN, Sorkin A. Inhibition of the receptor-binding function of clathrin adaptor protein AP-2 by dominant-negative mutant μ 2 subunit and its effects on endocytosis. *EMBO J.* 1999;18(9):2489-2499.
42. Mishra SK, Keyel PA, Edeling MA, Dupin AL, Owen DJ, Traub LM. Functional dissection of an AP-2 β 2 appendage-binding sequence within the autosomal recessive hypercholesterolemia protein. *J Biol Chem.* 2005;280(19):19270-19280.
43. Kelly BT, Graham SC, Liska N, et al. AP2 controls clathrin polymerization with a membrane-activated switch. *Science.* 2014;345(6195):459-463.
44. Aguet F, Antonescu Costin N, Mettlen M, Schmid Sandra L, Danuser G. Advances in analysis of low signal-to-noise images link dynamin and AP2 to the functions of an endocytic checkpoint. *Dev Cell.* 2013;26(3):279-291.
45. Kadlecova Z, Spielman SJ, Loerke D, Mohanakrishnan A, Reed DK, Schmid SL. Regulation of clathrin-mediated endocytosis by hierarchical allosteric activation of AP2. *J Cell Biol.* 2016;216(1):167-179.
46. Reis CR, Chen PH, Srinivasan S, Aguet F, Mettlen M, Schmid SL. Crosstalk between Akt/GSK3 β signaling and dynamin-1 regulates clathrin-mediated endocytosis. *EMBO J.* 2015;34(16):2132-2146.
47. Puthenveedu MA, von Zastrow M. Cargo regulates clathrin-coated pit dynamics. *Cell.* 2006;127(1):113-124.
48. Guo X, Mattera R, Ren X, et al. The adaptor protein-1 α subunit expands the repertoire of basolateral sorting signal recognition in epithelial cells. *Dev Cell.* 2013;27(3):353-366.

49. Hinrichsen L, Harborth J, Andrees L, Weber K, Ungewickell EJ. Effect of clathrin heavy chain- and alpha-adaptin-specific small inhibitory RNAs on endocytic accessory proteins and receptor trafficking in HeLa cells. *J Biol Chem*. 2003;278(46):45160-45170.
50. Motley A, Bright NA, Seaman MN, Robinson MS. Clathrin-mediated endocytosis in AP-2-depleted cells. *J Cell Biol*. 2003;162(5):909-918.
51. Fortian A, Dionne LK, Hong SH, et al. Endocytosis of ubiquitylation-deficient EGFR mutants via clathrin-coated pits is mediated by ubiquitylation. *Traffic (Copenhagen, Denmark)*. 2015;16(11):1137-1154.
52. Mettlen M, Loerke D, Yarar D, Danuser G, Schmid SL. Cargo- and adaptor-specific mechanisms regulate clathrin-mediated endocytosis. *J Cell Biol*. 2010;188(6):919-933.

SUPPORTING INFORMATION

Additional supporting information may be found online in the Supporting Information section at the end of this article.

How to cite this article: Mino RE, Chen Z, Mettlen M, Schmid SL. An internally eGFP-tagged α -adaptin is a fully functional and improved fiduciary marker for clathrin-coated pit dynamics. *Traffic*. 2020;21:603–616. <https://doi.org/10.1111/tra.12755>